Atmospheric Research 326 (2025) 108295

Contents lists available at ScienceDirect

Atmospheric Research

journal homepage: www.elsevier.com/locate/atmosres

Spatiotemporal variations in solar radiation due to aerosol and cloud radiative effects over the Korean Peninsula

Jung-Woo Yoo [a], Soon-Young Park [b], Jiseon Kim [c], Hyun-Goo Kim [d], Soon-Hwan Lee [a,e,*]

[a] Institute of Environmental Studies, Pusan National University, Busan 46241, Republic of Korea
[b] Department of Science Education, Daegu National University of Education, Daegu 42411, Republic of Korea
[c] Department of Earth Science, Pusan National University, Busan 46241, Republic of Korea
[d] Renewable Energy Institute, Korea Institute of Energy Research, Daejeon 34129, Republic of Korea
[e] Department of Earth Science Education, Pusan National University, Busan 46241, Republic of Korea

ARTICLE INFO

Keywords:
Solar radiation
Aerosol direct effect
Cloud radiative effect
Stratus
Cumulus

ABSTRACT

This study investigated the complex relationships between aerosols, clouds, and solar radiation over the Korean Peninsula using long-term observational data from 1994 to 2023. We identified a negative correlation between PM_{10} concentration and solar radiation, indicating that aerosol levels significantly affect solar energy availability. Using the WRF-CMAQ coupled model, we quantitatively analyzed the contributions of aerosol direct effect (ADE) and cloud radiative effect (CRE), focusing on the differing impacts of stratus and cumulus clouds. Our findings reveal that stratus clouds, which are prevalent in the early morning, contribute substantially to ADE, while cumulus clouds, which develop in the afternoon owing to increased surface heating, primarily influence CRE. The Seoul Metropolitan Area (SMA) showed the highest contributions from both ADE and CRE, indicating that areas with a high population density and elevated aerosol concentrations (PM_{10}, $PM_{2.5}$, and AOD) experienced a pronounced impact of ADE on solar radiation. Conversely, in the Gangwon (GW) region, where mountainous terrain promotes cumulus cloud development, the afternoon contributions of CRE are more pronounced. This analysis underscores the necessity of considering topographical and geographical characteristics and cloud formation timing when evaluating solar energy potential, providing valuable insights for future forecasting and site selection.

1. Introduction

Climate change poses a significant threat to ecosystems and human societies worldwide, primarily driven by greenhouse gas emissions. Addressing this issue necessitates the adoption of renewable energy sources, among which solar energy emerges as a clean, abundant, and sustainable resource. Solar power generation, in particular, emits minimal greenhouse gases such as CO_2, making it a highly advantageous option for mitigating climate change (Borenstein, 2008). In addition, compared to fossil fuels, solar energy offers substantial economic and environmental benefits while efficiently meeting daytime energy demands (Wild, 2009).

However, solar energy is significantly influenced by various atmospheric factors, such as aerosols and clouds, which impact the amount of solar radiation reaching the Earth's surface. Aerosols influence the Earth's radiation budget through both direct and indirect effects. The aerosol direct effect (ADE) refers to the scattering and absorption of solar radiation by aerosol particles (Charlson et al., 1992). Indirectly, aerosols modify cloud properties by increasing droplet number and decreasing droplet size (Twomey, 1974), and by suppressing precipitation, thereby extending cloud lifetime and enhancing cloud optical thickness (Albrecht, 1989; Pincus and Baker, 1994). These effects reduce the amount of solar radiation reaching the surface, thereby lowering the efficiency of solar power generation (Yoo et al., 2019; Yoo et al., 2020; Korras-Carraca et al., 2021; Papachristopoulou et al., 2022; Yoo et al., 2024). Furthermore, aerosol deposition on photovoltaic panels can degrade their performance by reducing transmittance and increasing maintenance requirements (Tanesab et al., 2019). For example, a study conducted in South Korea reported that aerosols reduce daytime solar radiation by approximately 50 $W \cdot m^{-2}$ (Yoo et al., 2019). Moreover, using MERRA-2 reanalysis data and spectral radiative transfer models, another study demonstrated that ADE decreases the global net solar

* Corresponding author at: Department of Earth Science Education, Pusan National University, Busan 46241, Republic of Korea.
E-mail address: withshlee@pusan.ac.kr (S.-H. Lee).

https://doi.org/10.1016/j.atmosres.2025.108295
Received 12 March 2025; Received in revised form 26 May 2025; Accepted 13 June 2025
Available online 18 June 2025
0169-8095/© 2025 Published by Elsevier B.V.

energy input by 5.21 $W \cdot m^{-2}$ (Korras-Carraca et al., 2021).

Clouds play a critical role in modulating solar radiation reaching the surface by reflecting and absorbing it. This phenomenon, known as the Cloud Radiative Effect (CRE), depends on cloud properties such as thickness, altitude, water content, and spatial distribution (L'Ecuyer et al., 2019; Liu et al., 2022). Clouds block solar radiation, significantly reducing surface solar irradiance, with a global average CRE effect of -24.8 ± 8.7 $W \cdot m^{-2}$ (L'Ecuyer et al., 2019). From a climatological perspective, clouds can reduce solar radiation more effectively than aerosols (Yamasoe et al., 2017; Dumka et al., 2021), with multilayered clouds and stratocumulus clouds exhibiting the most pronounced effects (L'Ecuyer et al., 2019). CRE's impact varies based on regional and seasonal meteorological conditions. For instance, He et al. (2024) reported that cloud type distributions cause small-scale fluctuations in surface solar radiation, which in turn lead to temporal and spatial variability in solar power generation. These fluctuations, when combined with cloud-induced radiative effects, can directly influence the overall efficiency of solar energy systems.

The impacts of ADE and CRE exhibit significant spatiotemporal variability, critically affecting the solar radiation reaching the surface. Yoo et al. (2019) found that the regional ADE varies depending on $PM_{2.5}$ concentrations, while Korras-Carraca et al. (2021) reported up to a tenfold difference in ADE between regions. Zhang et al. (2022) emphasized that ADE and CRE contribute to seasonal and regional variability in solar radiation, and Song et al. (2019) highlighted how changes in cloud properties influence aerosol radiative forcing, modifying spatial patterns. Che et al. (2018) demonstrated that aerosol optical properties and radiative forcing exhibit substantial regional variability in eastern China. The findings of these studies highlight the complex and spatiotemporal variability of the effects of aerosols and clouds on solar radiation.

Previous studies have analyzed the temporal variability of solar irradiance using satellite-based observations (Oh et al., 2024). However, these approaches rely on multiple assumptions for estimating solar irradiance and are subject to limitations such as the misclassification of clouds due to aerosol presence (Qu et al., 2017; Zhang et al., 2019; Zhang et al., 2020; Robbins et al., 2022). Moreover, total cloud cover observations cannot distinguish the individual effects of clouds and aerosols, making it challenging to accurately assess regional forecast performance. Recent studies have proposed methods for analyzing the variability of solar radiation and effectively separating direct and diffuse radiation components using machine learning algorithms such as deep learning (Oh et al., 2022; Oh et al., 2024). These approaches utilize observational datasets to enhance the spatial and temporal resolution of solar irradiance forecasts. However, deep learning-based prediction models are limited in their ability to directly simulate complex atmospheric processes, such as aerosol-cloud-radiation interactions. To overcome these limitations, it is essential to utilize numerical weather prediction models that can accurately quantify the contributions of aerosols and clouds to solar radiation. Coupled meteorology-air quality models provide a precise framework for simulating aerosol-cloud-radiation interactions, thereby improving the reliability of solar irradiance predictions and enabling a more detailed analysis of regional variations. This, in turn, facilitates the accurate forecasting of solar radiation and provides valuable insights for optimal photovoltaic site selection.

This study aims to analyze the spatiotemporal impacts of ADE and CRE on solar radiation over the Korean Peninsula using long-term meteorological and air quality observational data. Furthermore, this study employs a two-way coupled meteorological and air quality modeling system to quantitatively evaluate the contributions of aerosols and clouds. The analysis enhances the accuracy of solar energy forecasting and supports the optimal selection of photovoltaic deployment sites by considering spatiotemporal distributions.

2. Methods

2.1. Meteorological and air quality observational data

This study analyzed the trends in meteorological factors and air quality in Korea using long-term observational data from 1994 to 2023. To examine regional differences in ADE and CRE, Korea was divided into five regions: the Seoul Metropolitan Area (SMA), Gangwon (GW), Central, West, and East (Fig. 1). Meteorological data including solar radiation, sunshine duration, total cloud cover, precipitation, and cloud type were obtained from the Korea Meteorological Administration (KMA) Automated Synoptic Observing System (ASOS). The data collection sites for each region with long-term observational data were Seoul (SMA), Gangneung (GW), Daejeon (Central), Gwangju (West), and Busan (East) (indicated by red stars in Fig. 1). Annual averages were used for sunshine duration, cloud cover, and precipitation, and cumulative annual data were used for solar radiation. Because of the relocation of the cloud observation station from Gangneung to Bukgangneung, hourly data from the Bukgangneung station for the period 2009–2023 were analyzed. Air quality data (PM_{10} concentrations from 1996 to 2023) were obtained from the Air Quality Monitoring Station (AQMS) of the National Institute of Environmental Research using regionally averaged annual and monthly data.

To evaluate the performance of the meteorological model, hourly temperature, wind speed, and solar radiation data observed at 39 ASOS stations that measured solar radiation within the domain during the analysis period were used. For the evaluation of the air quality model results, PM_{10} concentration data from 320 AQMS stations were used.

2.2. Numerical models

In this study, the WRF-CMAQ two-way coupled system was used to analyze the impact of aerosols and clouds on solar radiation. This system integrates the Weather Research and Forecasting model (WRF, version 3.8) with the Community Multiscale Air Quality model (CMAQ, version 5.2). This model allows for aerosol feedback, particularly the direct aerosol effect, by incorporating shortwave radiation from the meteorological model and aerosol simulations from the air quality model (Wong et al., 2012). In this framework, key aerosol optical properties, including aerosol optical depth (AOD), single scattering albedo (SSA), and asymmetry factor (AF), are calculated within the CMAQ model and dynamically transferred to WRF. These parameters are used in the WRF shortwave radiation scheme to simulate aerosol-radiation interactions in real time, enabling an explicit representation of the aerosol direct effect (ADE) on surface solar irradiance. The modeling domain (Fig. 1) covers Korea with a 12 km horizontal resolution (260×240 grids) and 40 vertical layers. The initial and boundary conditions were provided by the Final Operational Global Analysis (FNL) reanalysis data, with a horizontal resolution of $0.25^\circ \times 0.25^\circ$. The detailed model configurations are summarized in Table S1. In the CMAQ model, biogenic emissions were estimated using the Model of Emissions of Gases and Aerosols from Nature (MEGAN, version 2.1). Anthropogenic emissions were obtained from two sources: international emissions were obtained from The Emissions Database for Global Atmospheric Research (EDGARv6.1; https://edgar.jrc.ec.europa.eu/dataset_ap61, last accessed June 2023), and domestic emissions were based on data from the Clean Air Policy Support System (CAPSS).

To examine the effects of aerosols and clouds on solar radiation, three simulations were conducted, as listed in Table 1: The BASE simulation, which includes both aerosol and cloud radiation feedback, served as a reference case for comparison with other simulations. In the NoADE (No Aerosol Direct Effect) simulation, the aerosol direct effect feedback is disabled, and the difference between the BASE and NoADE simulations highlights the influence of ADE on solar radiation. Similarly, the NoCRE (No Cloud Radiation Effect) simulation disables the cloud radiation effect option in the WRF model, and the differences between

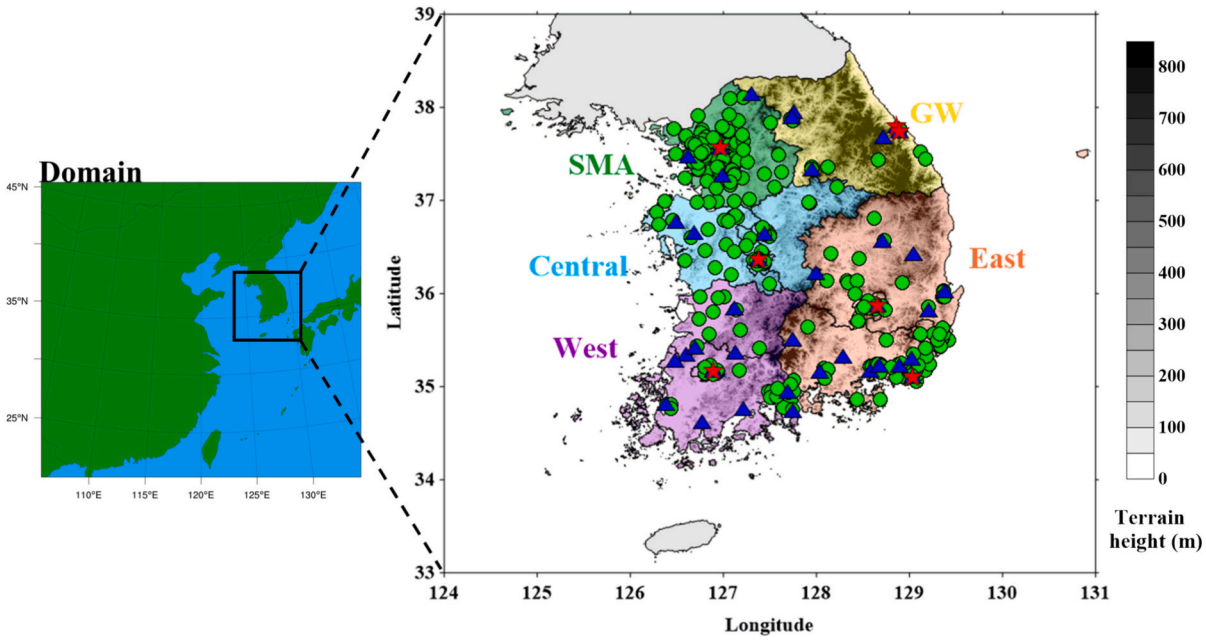

Fig. 1. Model domain illustrating the locations of meteorological observation stations (blue triangles) and air quality monitoring stations (green circles), along with the five shaded regions. (For interpretation of the references to colour in this figure legend, the reader is referred to the web version of this article.)

Table 1
Overview of the simulation scenarios conducted in this study.

Simulation	Aerosol direct effect	Cloud radiative effect
BASE	O	O
NoADE	X	O
NoCRE	O	X

the BASE and NoCRE simulations reveal the CRE on solar radiation.

3. Results

3.1. Analysis of observational data from 1994 to 2023

Fig. 2 presents an analysis of meteorological factors (cloud cover, sunshine duration, cumulative solar radiation, and precipitation) in Korea from 1994 to 2023, along with PM_{10} concentrations from 1996 to 2023. To examine long-term trends, the data were analyzed at the following 10-year intervals: 1994–2003, 2004–2013, and 2014–2023. PM_{10} was selected as the indicator of aerosol concentrations for this analysis, given its longer observational record compared to $PM_{2.5}$. These results are crucial for understanding the impacts of aerosols and meteorological factors on solar radiation. Over the past 30 years, PM_{10} concentrations have shown an overall decreasing trend, with a notable 25 % reduction observed in the last decade (2014–2023) compared to 2004–2013 (Fig. 2a). This reduction can be attributed to the positive effects of the emission reduction policies implemented by the Korean government, as mentioned in previous research (Kim and Lee, 2018). The decrease in PM_{10} concentrations likely led to a reduction in ADE, resulting in an increase in surface solar radiation. Over the last decade (2014–2023), solar radiation and sunshine duration increased by approximately 6 % and 11 %, respectively (Fig. 2e, f). Monthly PM_{10} concentrations peaked in spring (March, April, Mar), with the highest concentration observed in March (66 $\mu g \cdot m^{-3}$), indicating that aerosols can significantly reduce solar radiation during this season. Cloud cover has increased slightly by 1 % over the past 30 years, with no significant long-term trend observed (Fig. 2c). While cumulative precipitation decreased from 2014 to 2023 (Fig. 2d), solar radiation and sunshine duration increased (Fig. 2e, f). While cloud cover exhibited a slight increase and precipitation showed a decreasing trend, these changes alone do not seem to account for the observed increase in surface solar radiation. Rather, the overall reduction in PM_{10} concentrations appears to have played a more influential role, likely as a result of recent emission control efforts. Aerosols scatter and absorb solar radiation, thereby reducing the amount that reaches the surface. As PM_{10} concentrations declined, the associated attenuating effect on solar radiation weakened, resulting in increased surface solar radiation. For example, during 2004–2013, a 5.5 % decrease in PM_{10} concentrations did not correspond to a noticeable change in sunshine duration. In contrast, between 2014 and 2021, a 25 % decrease in PM_{10} concentrations was associated with an 11 % increase in sunshine duration. This inverse relationship is consistent with previous findings (Lee et al., 2022), which highlight the positive impact of aerosol reduction on solar radiation. Nonetheless, the complex interactions among aerosols, clouds, and precipitation can vary depending on cloud type and seasonal meteorological conditions, indicating the need for further quantitative assessment to accurately isolate each contribution.

Solar energy generation is highly influenced by changes in solar radiation. With the reduction in ADE due to lower PM_{10} concentrations, solar radiation increased, potentially improving the efficiency of solar power generation. Over the past 30 years (1994–2023), cloud cover has not exhibited a statistically significant long-term trend, suggesting that its contribution to the observed increase in surface solar radiation is likely limited. This indicates that the increase in solar radiation may be more closely related to reductions in aerosol loading, particularly the decline in PM_{10} concentrations. Nevertheless, cloud cover plays a critical role in modulating solar radiation. Different types of clouds can either block or scatter incoming sunlight, thereby influencing the amount of solar radiation reaching the surface (L'Ecuyer et al., 2019; He et al., 2024). Previous studies have shown that clouds often exert a more pronounced influence on solar radiation than aerosols (Yamasoe et al., 2017; Dumka et al., 2021). Therefore, while cloud cover may not have significantly contributed to long-term solar radiation trends, its radiative effects, along with those of aerosols, can still impact the efficiency of solar energy systems. Therefore, while cloud cover may not have significantly contributed to long-term solar radiation trends, its radiative effects, alongside those of aerosols, can still impact the efficiency of solar energy systems.

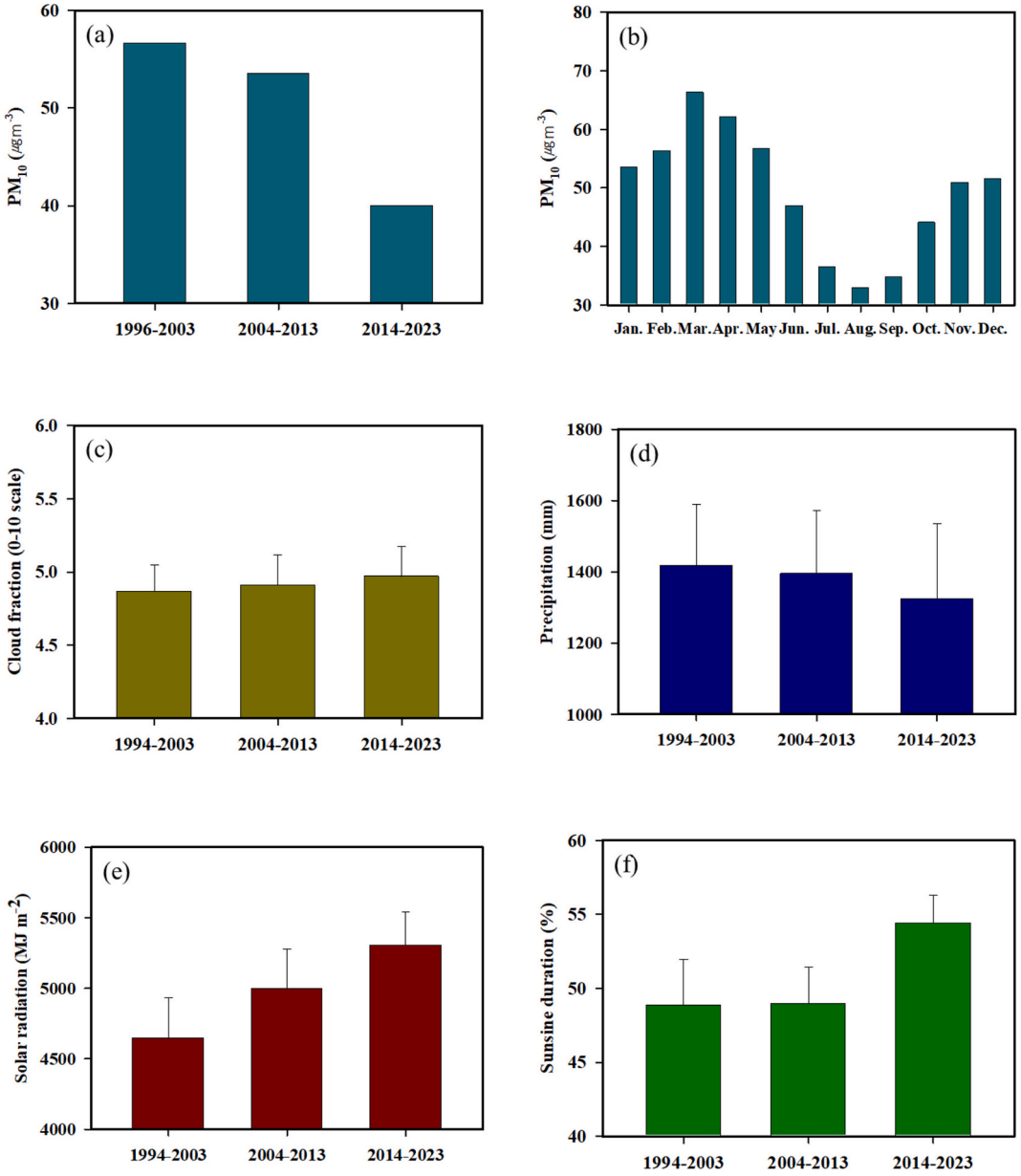

Fig. 2. Long-term trends of (a) PM_{10}, (b) monthly PM_{10}, (c) cloud cover, (d) annual cumulative precipitation, (e) annual cumulative solar radiation, and (f) sunshine duration.

To this end, this study focused on analyzing the impact of aerosols and clouds on solar radiation over the Korean Peninsula in March 2019, which was selected based on long-term observational data showing that monthly PM_{10} (Fig. 2b) and $PM_{2.5}$ (Fig. S1b) concentrations peaked in March, averaging 66 $\mu g \cdot m^{-3}$ and 30 $\mu g \cdot m^{-3}$, respectively. In particular, March 2019 recorded high concentrations of PM_{10} (62 $\mu g \cdot m^{-3}$) and $PM_{2.5}$ (39 $\mu g \cdot m^{-3}$), making it one of the most polluted March periods in recent years. Importantly, this period was not influenced by dust storm events, ensuring that the elevated aerosol loading was predominantly anthropogenic. Based on these considerations, March 2019 was selected as the case study period for assessing the spatiotemporal impacts of aerosol-cloud-radiation interactions on solar energy availability over the Korean Peninsula.

3.2. Model validation

To evaluate the accuracy of the WRF simulations for solar radiation and meteorological factors, the performance of the model was assessed against 39 Automated Synoptic Observing System (ASOS) sites across Korea, where solar radiation is measured (Table 2). The evaluation focused on data from March 2019, and the meteorological factors assessed were the 2-m air temperature (T2), 10-m wind speed (WS10), solar radiation, and total cloud cover using hourly data.

For air temperature (T2), the Index of Agreement (IOA) and correlation coefficient (R) were 0.87 and 0.83, respectively, indicating that the model captured the diurnal variability well, though a slight

Table 2
Statistical validation results of simulated and observed T2, WS10, solar radiation, CF, and PM_{10}.

	Obs. mean	Model mean	MB	IOA	R
T2 (°C)	7.59	5.52	−2.07	0.87	0.83
WS10 ($m \cdot s^{-1}$)	2.32	3.45	1.13	0.70	0.58
Solar radiation ($MJ \cdot m^{-2}$)	1.15	1.38	0.23	0.83	0.72
CF (0–10 scale)	4.83	5.30	0.47	0.75	0.54
PM_{10} ($\mu g \cdot m^{-3}$)	63.89	43.04	−20.85	0.67	0.53

underestimation was observed with a mean bias (MB) of −2.07 °C. Wind speed (WS10) was overestimated by 1.13 $m \cdot s^{-1}$ compared to observations, but the IOA and R were 0.70 and 0.58, respectively, showing that the model simulated winds reasonably well. Despite the tendency to underestimate temperature, overall simulation results for temperature and wind speed met the baseline criteria proposed by Emery et al. (2001) (T2: Bias $\leq \pm 0.5$ °C; IOA ≥ 0.7, WS10: Bias ≤ 2.0 $m \cdot s^{-1}$; IOA ≥ 0.6). Regarding solar radiation and cloud cover, which are critical for solar energy generation, the model tended to slightly overestimate both compared to the observations. However, the IOA (R) for solar radiation was 0.83 (0.72), and for cloud cover, it was 0.75 (0.54), indicating reasonable accuracy. The overestimation of cloud cover in the WRF model may be due to limitations in cloud microphysical schemes.

Additionally, the CMAQ simulation results for PM_{10} concentrations were compared to hourly measurement data from 320 AQMS sites. Although the simulation tended to underestimate PM_{10} levels, an IOA of 0.67 indicated that the model effectively captured the variability of PM_{10} concentrations. The inaccuracy of the air quality simulation results could be attributed to uncertainties in the anthropogenic emissions data, initial and boundary conditions, and the meteorological model output (Miao et al., 2017). Overall, the good agreement between the simulation results and the observations suggests that the model is suitable for analyzing the impact of aerosols and clouds on solar radiation in Korea.

3.3. Cloud and aerosol distribution

Fig. 3 presents the spatial distributions of the average cloud fraction (CF), PM_{10}, and aerosol optical depth (AOD) simulated from the BASE simulations conducted for March 2019. To supplement the representation of aerosol characteristics, the spatial distribution of $PM_{2.5}$ is presented in the supplementary material (Fig. S2). According to Li et al. (2024), orographic uplift on the windward side of mountainous areas enhances updrafts and intensifies the cloud and precipitation processes, leading to increased cloud cover. In our study, CF values greater than 6 were observed in regions located on the windward side of high-altitude mountainous areas, specifically to the west of the GW region, east of the central region, and south of the western region. In Korea, March is influenced by northwesterly winds, which promote active cloud formation along the windward slopes of mountain ranges. This is because of the enhanced updrafts caused by orographic effects, which lift air as it ascends mountainous terrain, cooling and forming clouds more frequently. Consequently, cloud formation was concentrated in March in these areas because of the strengthened updrafts caused by the terrain.

The spatial distributions of PM_{10}, $PM_{2.5}$, and AOD were relatively high in western SMA and the western regions. This can be attributed to the higher population density and anthropogenic emissions in these areas (Yoo et al., 2019). Similar spatial distributions were observed by Jun and Gu (2023), who reported high $PM_{2.5}$ concentrations in Seoul and western Korea in March 2019. These high aerosol concentrations (PM_{10} and $PM_{2.5}$, and AOD) are primarily attributed to the long-range transport of air pollutants from foreign countries, which is consistent with the findings of this study.

To assess the validity of the results of this study, we compared the AOD values derived from MERRA-2 reanalysis data with those simulated using the CMAQ model. MERRA-2 provides AOD data at a spatial resolution of 0.5° × 0.625° and a temporal resolution of 3-h intervals (Fig. S3). For comparison, the March AOD values from both datasets were averaged. Although the CMAQ model tended to slightly underestimate AOD compared to MERRA-2, it successfully captured the spatial distribution, with higher AOD values over the SMA and western Korea and lower values over the eastern regions. In contrast, MERRA-2 showed an elevated AOD over the Yellow Sea (West Sea), which is indicative of the long-range transport of aerosols. However, this underrepresented the high AOD levels linked to domestic emissions in Korea. The high-resolution CMAQ results highlighted regions of high AOD driven by local emissions more effectively (Fig. 3). Furthermore, the CMAQ model reflects the spatial distribution of aerosols across the Korean Peninsula more accurately, allowing us to better identify regions where the effects of ADE and CRE are pronounced. Through this analysis, the combination of CF and aerosol (PM_{10}, $PM_{2.5}$, and AOD) spatial distributions from numerical models helps identify areas where aerosols and clouds interact significantly, providing deeper insights into regional variations in ADE and CRE.

3.4. Solar radiation distribution

Fig. 4 presents the spatial distributions of accumulated surface solar radiation (SSR), direct solar radiation (SSR_DIR), and diffuse solar radiation (SSR_DIF) over the Korean Peninsula for March 2019. Direct solar radiation refers to solar energy that reaches the surface without being scattered or absorbed by aerosols or clouds. It was generally higher under clear skies with minimal cloud cover. Conversely, high aerosol concentrations or thick cloud cover can significantly reduce direct solar radiation. While diffuse radiation generally increases on

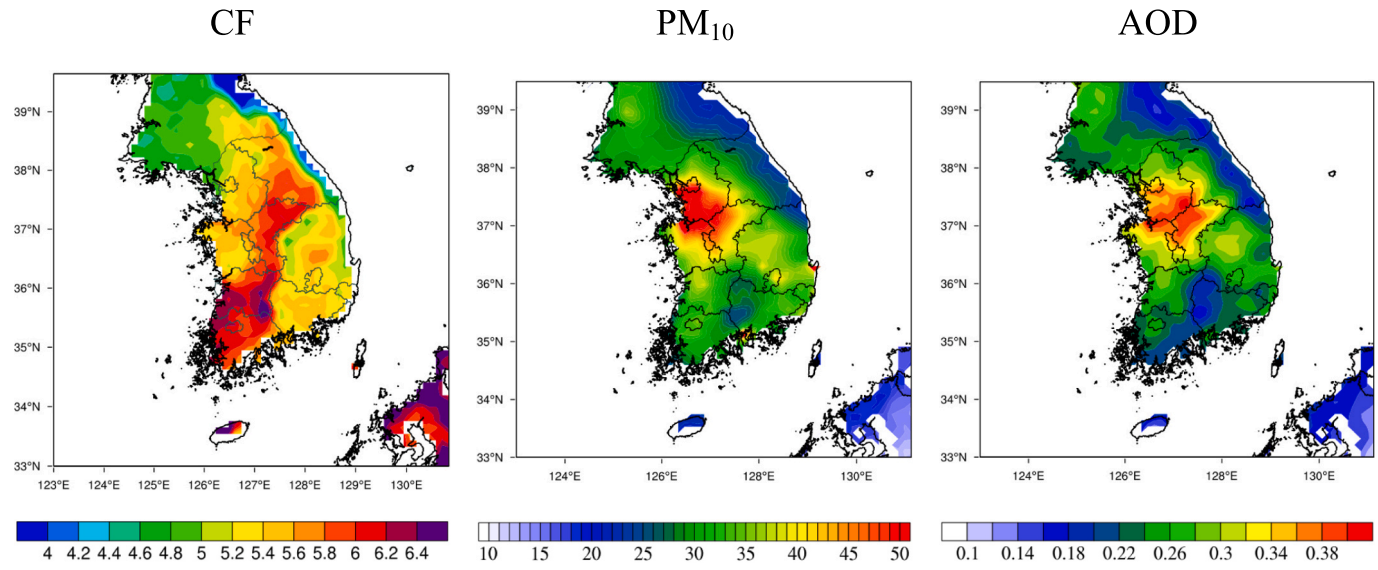

Fig. 3. Spatial distributions of monthly average cloud fraction (CF, 0–10 scale), PM_{10} ($\mu g \cdot m^{-3}$), and aerosol optical depth (AOD) for BASE simulation during March 2019.

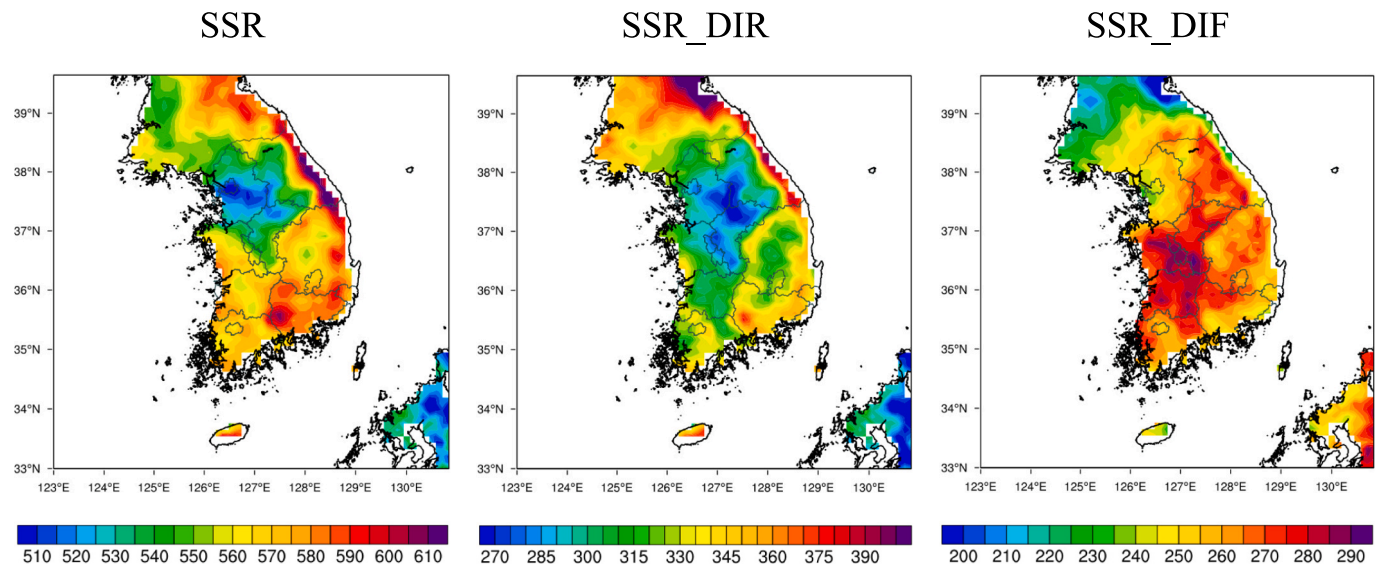

Fig. 4. Spatial distributions of cumulative surface solar radiation (SSR), cumulative direct shortwave radiation (SSR_DIR), and cumulative diffuse shortwave radiation (SSR_DIF) for BASE simulation during March 2019.

days with higher aerosol concentrations or moderate cloud cover due to enhanced scattering, both diffuse and direct solar radiation can decrease significantly under very thick cloud conditions because of strong attenuation.

The spatial pattern of SSR_DIR results from the impacts of both the ADE and CRE, as represented in the BASE simulation. This suggests that aerosols and clouds significantly reduce solar radiation in these areas. In contrast, regions with higher topography, such as the eastern GW and the eastern region, recorded relatively higher SSR_DIR. Mountainous terrains promote orographic lifting, which cools the air and enhances cloud formation. Consequently, cloud formation is more active on the windward side of the mountains, reducing radiation, whereas the descending air on the leeward side is relatively dry, leading to clearer skies. For SSR_DIF, lower values were observed in the SMA, where aerosol concentrations were higher, whereas regions with more cloud cover showed increased SSR_DIF, which corresponded to the spatial cloud fraction distribution shown in Fig. 3. Previous studies have reported that under broken-cloud conditions, solar radiation can be reflected from the sides of clouds, increasing the amount of radiation reaching the surface (Pfister et al., 2003; Emck and Richter, 2008; Berg et al., 2011; de Andrade and Tiba, 2016). This suggests that clouds play a major role in solar radiation scattering.

In conclusion, regions with high aerosol concentrations exhibited reduced SSR_DIR values due to ADE. Areas with significant cloud cover showed an increase in SSR_DIF, likely due to cloud scattering effects. However, the spatial distributions of CF and AOD alone are insufficient to fully explain the observed variations in SSR, SSR_DIR, and SSR_DIF. Therefore, further numerical model simulations are required to quantitatively assess the relative contributions of ADE and CRE. Such analyses will enhance our understanding of solar radiation variability and the quantitative impacts of aerosols and clouds on solar radiation.

3.5. Aerosol and cloud effects

Fig. 5 shows the impacts of ADE and CRE on accumulated SSR, SSR_DIR, and SSR_DIF in March. Overall, due to the influence of aerosols and clouds, both SSR and SSR_DIR decreased, whereas SSR_DIF increased; however, their spatial distributions varied. The direct effect of aerosols led to average decreases in SSR and SSR_DIR of -33 MJ·m^{-2} (-6 %) and -64 MJ·m^{-2} (-20 %), respectively (Table 3). The reduction in solar radiation was particularly pronounced in regions with high AOD, such as the southeastern SMA region and the central eastern part of the Korean Peninsula. In contrast, SSR_DIF increased by an average of $+30$ MJ·m^{-2} ($+13$ %) due to aerosol scattering, which caused the sunlight to spread in multiple directions, reaching the surface after being scattered in the atmosphere. The effect of clouds (CRE) followed a pattern similar to that of aerosols (ADE), but the impact was more significant. In regions with high cloud cover, such as GW and the eastern West region and East region, SSR and in SSR_DIR decreased by -113 MJ·m^{-2} (-20 %) and -224 MJ·m^{-2} (-70 %), respectively, as clouds more effectively blocked solar radiation. However, in areas with significant cloud cover, SSR_DIF increased by an average of $+110$ MJ·m^{-2} ($+46$ %), with the scattering effect of clouds particularly strong in high-altitude regions like GW and the West region.

Temporal variability is a key factor in solar power generation forecasting (Oh et al., 2022), and the impact of ADE and CRE exhibit distinct differences between daytime and nighttime. In the BASE simulation, which includes both aerosol and cloud radiative effects, daytime temperatures were generally lower than those in the NoADE and NoCRE simulations (Fig. 6 and Table S2), likely due to reductions in surface solar radiation from both aerosol scattering/absorption and cloud albedo shading. However, the nighttime thermal response differs between CRE and ADE. Clouds contribute significantly to nighttime warming by absorbing and reemitting longwave radiation, thereby mitigating radiative cooling near the surface. In the NoCRE simulation, where this effect is removed, more rapid surface cooling occurred, resulting in the lowest nighttime average temperature (1.81 °C) and the largest diurnal temperature range (8.10 °C) among the simulations.

By contrast, the NoADE simulation retained the cloud radiative effect, allowing the nocturnal warming influence of clouds to persist. Accordingly, nighttime temperatures in the NoADE simulation were relatively higher (3.34 °C), and the diurnal temperature range was smaller (6.93 °C), despite elevated daytime temperatures resulting from the absence of aerosol-induced solar attenuation. This led to a higher monthly mean 2-m temperature in NoADE (6.51 °C) compared to NoCRE (5.53 °C), even though CRE had a greater overall effect on reducing surface solar radiation than ADE. These results underscore the distinct radiative roles of clouds during the day and night, as they reduce incoming shortwave radiation in the daytime while absorbing and reemitting longwave radiation at night. These contrasting radiative effects of clouds during day and night clarify the temperature response patterns seen in the model simulations.

Although nighttime cloud effects do not directly alter daytime solar radiation, their modulation of nighttime surface cooling and subsequent

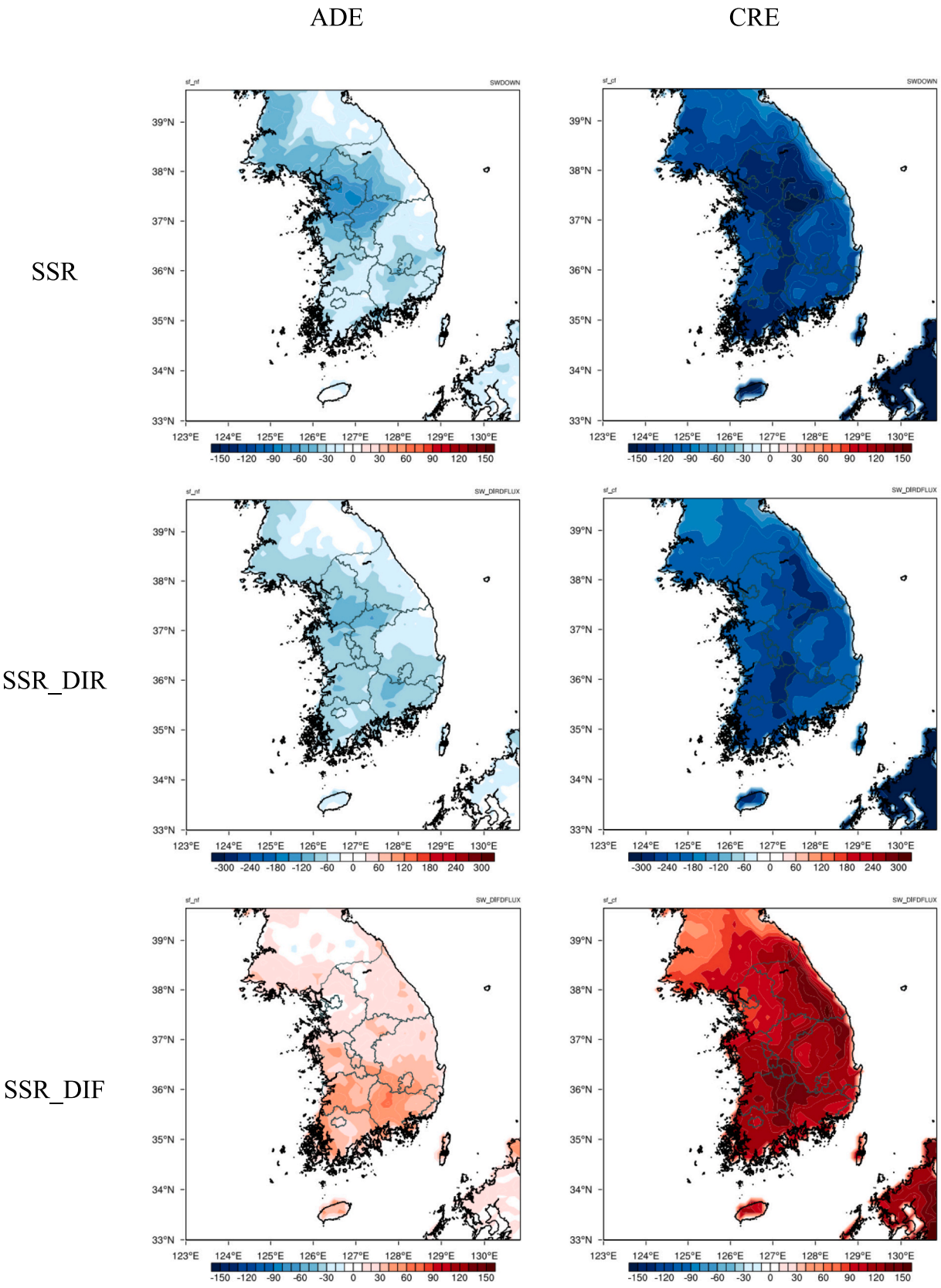

Fig. 5. Spatial distributions of the aerosol direct effects (ADE) and cloud radiation feedback (CRE) on surface solar radiation (SSR, MJ·m^{-2}), direct radiation (SSR_DIR, MJ·m^{-2}), and diffuse radiation (SSR_DIF, MJ·m^{-2}) during March 2019.

Table 3
Averaged cumulative surface solar radiation (SSR), cumulative direct shortwave radiation (SSR_DIR), and cumulative diffuse shortwave radiation (SSR_DIF) in BASE simulation and ADE aerosol direct effects (ADE) and cloud radiation feedback (CRE).

	BASE	ADE	CRE
SSR	553 MJ·m^{-2}	−33 MJ·m^{-2}	−113 MJ·m^{-2}
SSR_DIR	318 MJ·m^{-2}	−64 MJ·m^{-2}	−224 MJ·m^{-2}
SSR_DIF	238 MJ·m^{-2}	+30 MJ·m^{-2}	+110 MJ·m^{-2}

boundary layer development can influence early morning atmospheric conditions, potentially affecting solar irradiance and the predictability of solar energy generation. Therefore, understanding the diurnal thermal response shaped by CRE and ADE is essential for improving solar power forecasting accuracy. These findings also demonstrate that aerosols and clouds influence both the magnitude and composition of surface solar radiation by reducing direct solar radiation (SSR_DIR) and increasing diffuse radiation (SSR_DIF), and they additionally affect the diurnal temperature cycle and atmospheric stability. Neglecting these effects may lead to an overestimation of solar power generation, particularly in regions with high AOD or frequent cloud cover, thereby decreasing forecasting accuracy and operational reliability.

3.6. Effects of ADE and CRE under different cloud types

3.6.1. Cloud types

In the previous analysis (Section 3.5), it was observed that the impacts of ADE and CRE varied between daytime and nighttime owing to differences in cloud cover and radiative cooling. These effects are also influenced by cloud type. This section explores how ADE and CRE differ according to the cloud type. Generally, clouds can be categorized into two main types: stratus and cumulus clouds. Stratus clouds are thin, widespread clouds formed at lower altitudes and typically result from the cooling of surface air via radiative cooling. These clouds primarily form at night or during early morning, peaking their impact on solar radiation during the early morning (Eastman and Warren, 2014). On the other hand, cumulus clouds are vertically developed clouds that form during the afternoon when surface heating is the greatest due to solar radiation. Cumulus clouds have a significant influence on solar radiation during the midday and afternoon. Thus, cloud formation times differ based on cloud type, as do their impacts on solar radiation. This necessitates an analysis of ADE and CRE based on cloud type. Fig. 7 shows the hourly frequency of stratus and cumulus cloud occurrences from 2009 to 2023 as observed at the meteorological sites (indicated by red stars in Fig. 1). The results revealed that stratus clouds increase in

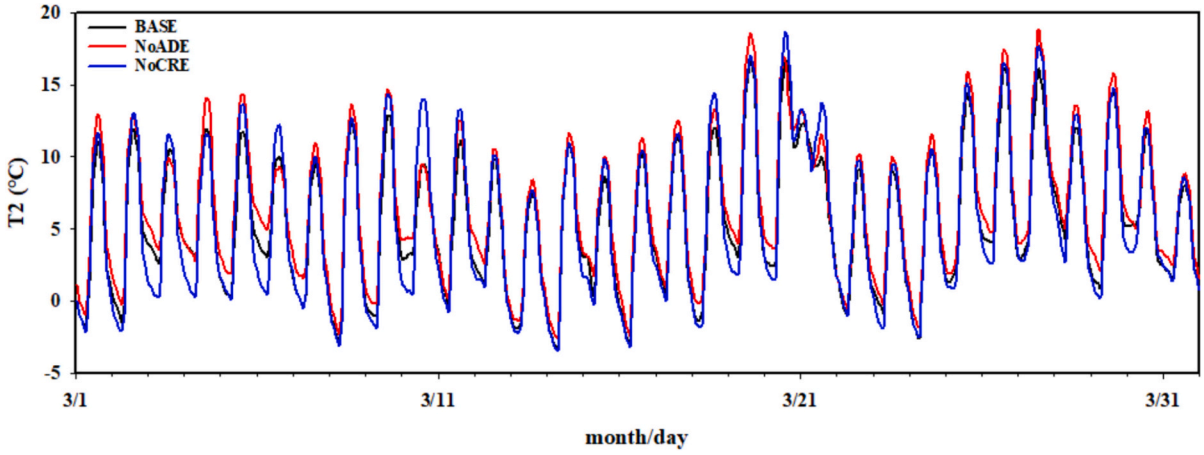

Fig. 6. Time series of 2-m average temperature (T2) from the BASE, NoADE, and NoCRE simulations during March 2019.

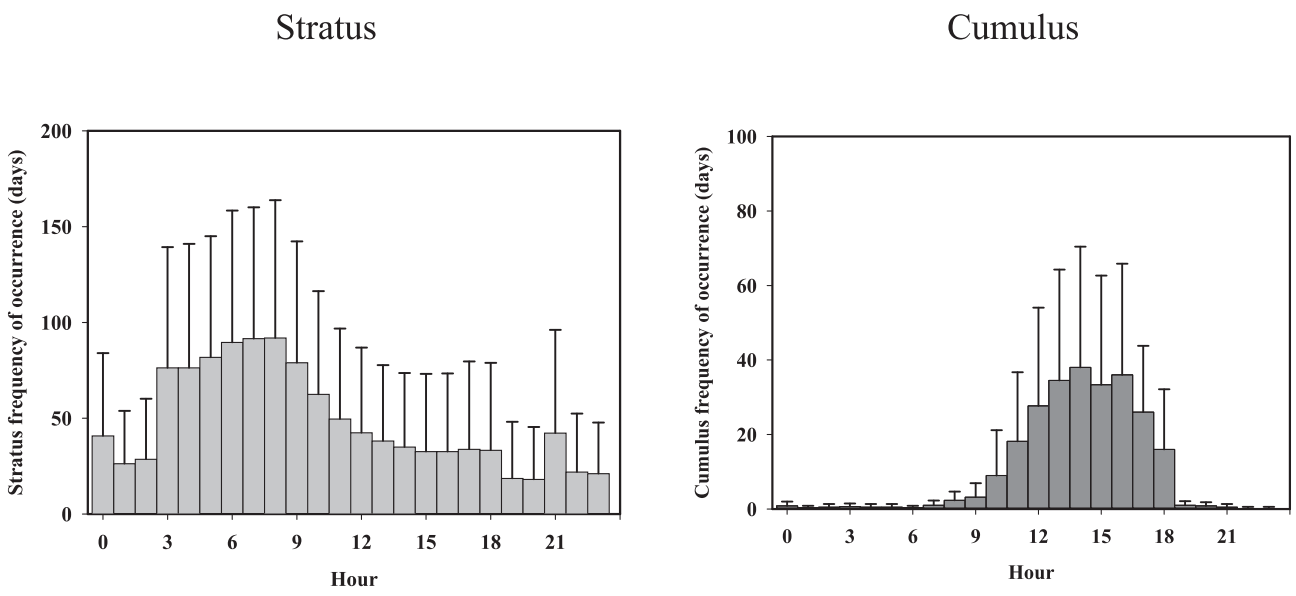

Fig. 7. Hourly average occurrence frequencies of stratus and cumulus clouds observed at meteorological stations (indicated in Fig. 1) from 2009 to 2023.

frequency starting at approximately 03:00 LST, peaking at 08:00 LST, and then gradually decrease. In contrast, cumulus clouds begin to increase in frequency around 11:00 LST, reaching their maximum at 14:00 LST. These differences in cloud type mechanisms and timings indicate that stratus and cumulus clouds distinctly affect solar radiation throughout the day. Understanding these differences is essential to interpret the impacts of ADE and CRE.

3.6.2. *Spatial and temporal variability in cloud occurrence and its influence on ADE and CRE*

Cloud formation varies not only temporally but also owing to regional topographical and geographical characteristics. In this section, we analyze the spatial and temporal differences in ADE and CRE, along with their impacts on solar radiation. To better understand this, we categorized our analysis based on the time of day when stratus clouds (07:00–09:00 LST) and cumulus clouds (14:00–16:00 LST) were most frequent. As the total amount of solar radiation varies depending on both the time and location of cloud formation, we calculated the contributions of ADE and CRE during these periods across different regions to compare their spatial and temporal effects. The contributions were determined using the following equation:

$$\text{Contribution} = \frac{SW - SW_i}{SW} \times 100(\%)$$

Where SW refers to the average solar radiation from the BASE simulation, and SW_i represents the daytime-averaged solar radiation from the NoADE and NoCRE simulations. Since this equation yields negative values to represent the reduction in solar radiation, all contribution values were presented as absolute values to emphasize the magnitude of the reduction and to enhance visual clarity. This approach allows for a clearer comparison of how ADE and CRE influence solar radiation at different times of the day.

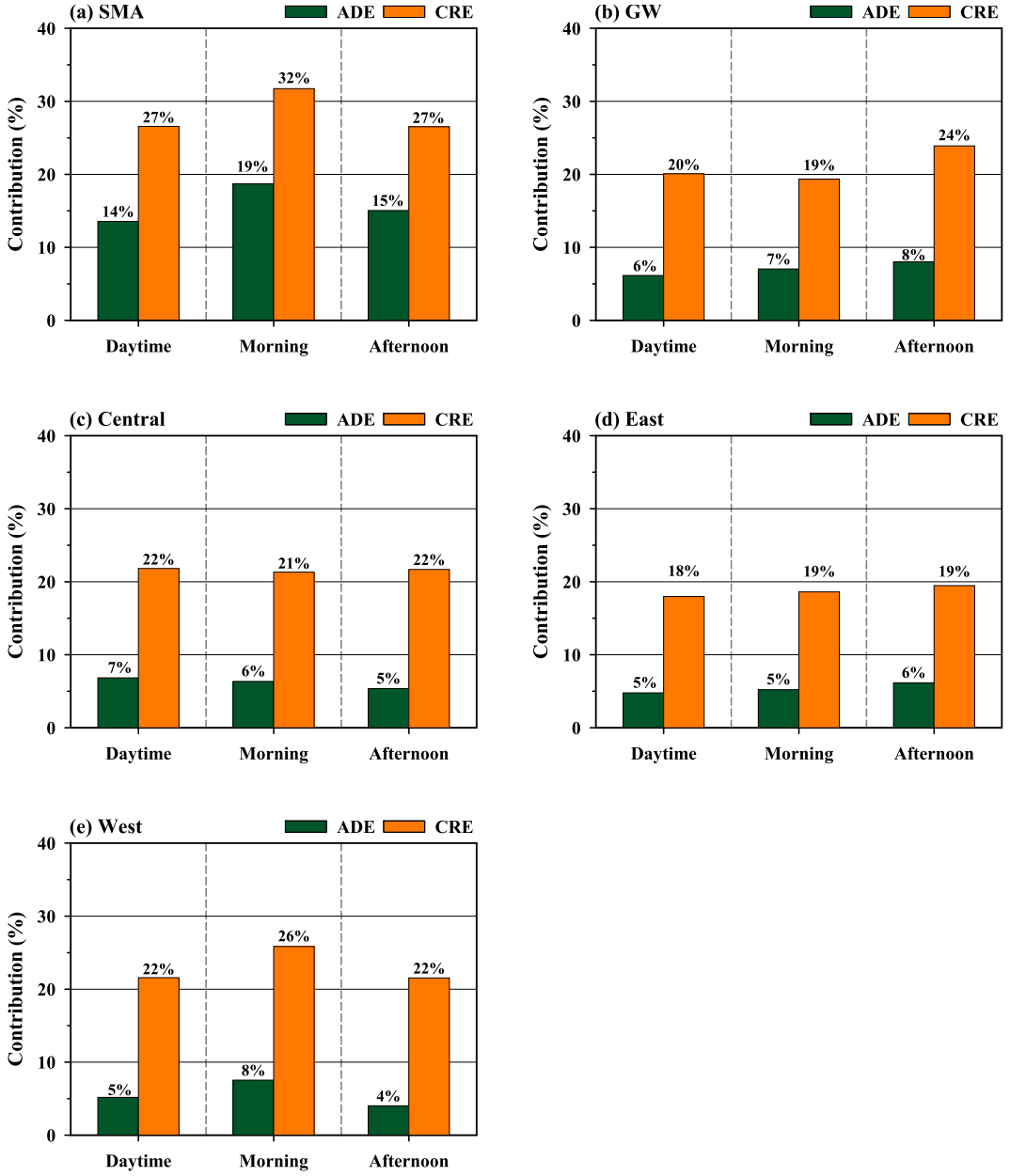

Fig. 8. Mean contributions of the aerosol direct effect (ADE) and cloud radiative effect (CRE) to the reduction in surface solar radiation during the daytime (07:00–17:00 LST), morning (07:00–09:00 LST), and afternoon (14:00–16:00 LST) in March 2019, across five regions: the Seoul Metropolitan Area (SMA), Gangwon (GW), Central, East, and West.

Fig. 8 illustrates the regional contributions of ADE and CRE to solar radiation during the daytime period (07:00–19:00 LST), the morning (07:00–09:00 LST) when stratus clouds were most prevalent, and the afternoon (14:00–16:00 LST) when cumulus clouds were most frequent. Significant reductions in solar radiation were observed across all periods, with the largest impacts in the SMA region, where ADE and CRE contributed 14 % and 27 %, respectively, indicating stronger attenuation of solar radiation compared to other regions.

In the SMA, the CRE contribution was greater in the morning (32 %) than in the afternoon (27 %). Conversely, in the GW region, the CRE contribution was greater in the afternoon (24 %) than in the morning (19 %). Although stratus clouds exhibited higher absolute frequency than cumulus clouds even in the afternoon (Fig. 7), the stronger afternoon CRE in the GW region is likely due to the presence of optically thicker cumulus clouds. These clouds are formed through enhanced convective activity driven by surface heating over mountainous terrain, which is characteristic of the GW region. According to Demko et al. (2009), cumulus clouds tend to form more frequently around midday in mountainous areas due to terrain-induced circulation. Therefore, when interpreting CRE, it is essential to consider cloud type and optical properties, not just occurrence frequency. The ADE contribution was approximately 4 % greater in the morning than in the afternoon in both the SMA and western regions. This was linked to higher AOD concentrations during the morning, particularly in the SMA, where maximum AOD levels occurred in the early hours (Fig. S4), resulting in more substantial ADE-induced attenuation of solar radiation.

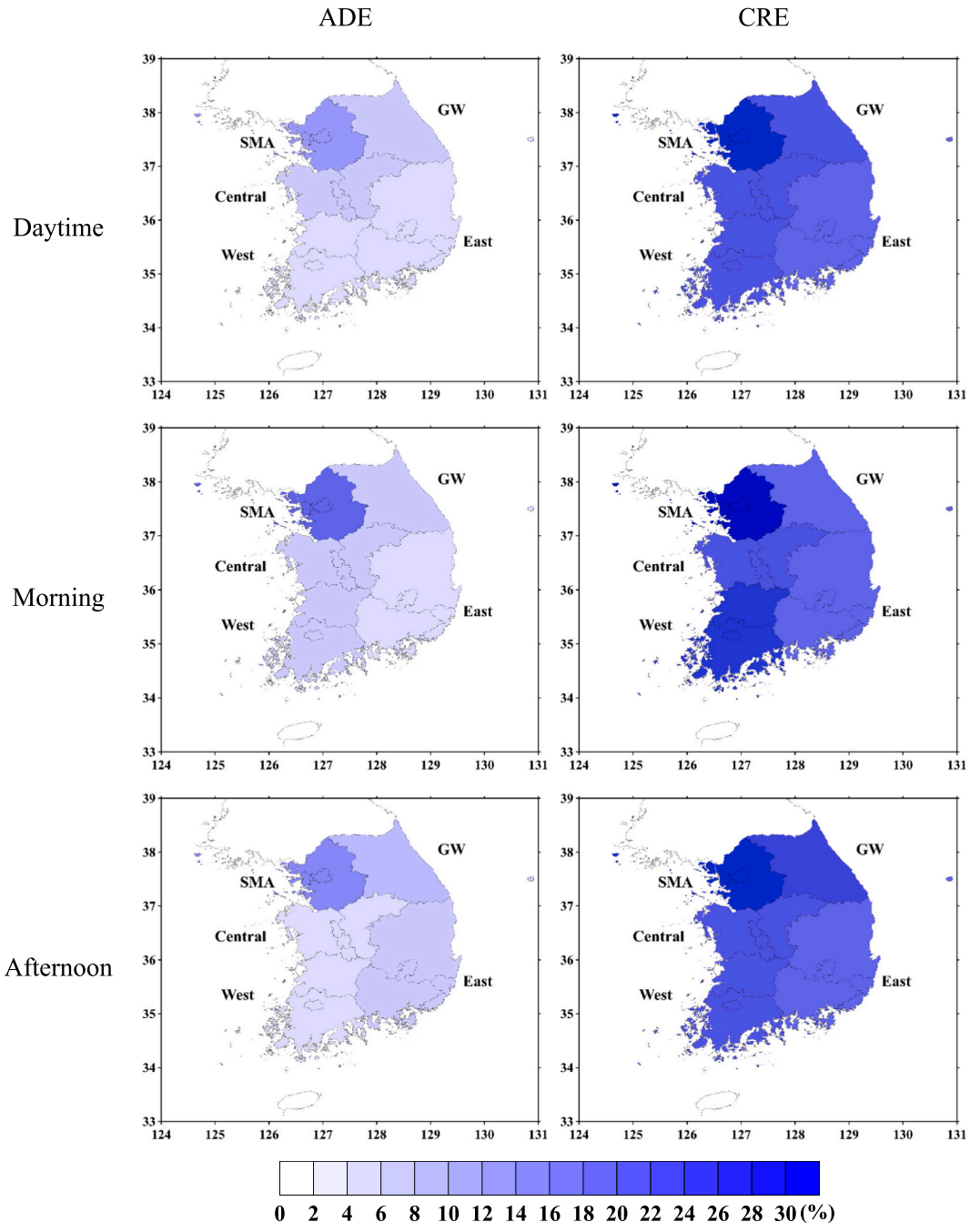

Fig. 9. Spatial distributions of the contributions of the aerosol direct effect (ADE) and cloud radiative effect (CRE) to the reduction in the surface solar radiation during the daytime (07:00–17:00 LST), morning (07:00–09:00 LST), and afternoon (14:00–16:00 LST) in March 2019, across five regions: the Seoul Metropolitan Area (SMA), Gangwon (GW), Central, West, and East.

Consequently, both aerosols and clouds contributed to the reduction in surface solar radiation, with their impacts exhibiting distinct spatial and temporal variations (Fig. 9). The highest contributions of both ADE and CRE were observed in the SMA region, which also exhibited the greatest population density and AOD levels. Temporally, their influence in the SMA was more pronounced in the morning (07:00–09:00 LST), aligning with the higher frequency of stratus clouds. In contrast, in the GW region, characterized by complex mountainous terrain, cumulus clouds were more frequent in the afternoon (14:00–16:00 LST), leading to a stronger CRE impact during that period. The orographic features and elevated topography of the region enhance surface heating and promote convective uplift, which are favorable conditions for afternoon cumulus cloud development.

Given these spatial and temporal differences, variability in aerosols and clouds can cause imbalances in solar energy generation, potentially intensifying the Duck Curve phenomenon. For instance, in the SMA region, the frequent occurrence of stratus clouds in the morning may suppress solar power output, complicating efforts to manage midday electricity surplus. Conversely, in the GW region, afternoon cumulus development leads to increased solar radiation variability, contributing to greater uncertainty in solar power forecasts. Consequently, understanding the spatiotemporal impacts of ADE and CRE can enhance the accuracy of solar power generation forecasts and provide valuable insights for optimal site selection in solar energy planning.

4. Conclusion

In this study, we analyzed long-term observational data (1994–2023) to confirm the negative correlation among PM_{10} concentrations, solar radiation, and sunshine duration across the Korean Peninsula. This finding indicates that solar radiation can vary with the aerosol concentration (PM_{10}, $PM_{2.5}$, and AOD). We focused on March 2019, a month characterized by high PM_{10} and $PM_{2.5}$ levels, to quantitatively assess the impacts of ADE and CRE on solar radiation using the WRF-CMAQ coupled model. Overall, the analysis revealed that both ADE and CRE contributed to a decrease in solar radiation and direct solar radiation while increasing diffused solar radiation. Notably, in the NoCRE simulation, nighttime temperatures were the lowest, which was attributed to greater cooling of the surface due to the absence of clouds compared with other simulations. Regionally, the effects of ADE and CRE were more pronounced in the SMA, where high population density and significant anthropogenic emissions led to marked reductions in solar radiation, particularly in the morning (07:00–09:00 LST), when AOD concentrations were elevated. In contrast, the GW region, characterized by higher elevation and mountainous terrain, exhibited the greatest influence of the CRE in the afternoon (14:00–16:00 LST), when cumulus cloud formation was frequent. These results suggest that the contributions of ADE and CRE to solar radiation can vary significantly based on topographical features and spatial and temporal distributions of aerosols and clouds.

This study provides critical insights into the spatial and temporal effects of aerosols and clouds on solar radiation using a meteorological-air quality coupled model, offering valuable implications for solar energy forecasting and site selection. By quantifying the contributions of ADE and CRE, this study assessed the atmospheric and meteorological suitability of various regions for solar energy deployment from an environmental perspective. However, practical solar energy site selection must also consider additional factors, including terrain, population density, grid infrastructure, and land-use constraints. As such, this study does not aim to directly recommend specific sites, but rather provides a scientific foundation for considering environmental factors in solar development planning.

Furthermore, while this study focused on a short-term simulation period due to computational limitations, it highlights the importance of long-term assessments that encompass seasonal and interannual variability. Future research should aim to conduct long-term simulations considering annual and seasonal variations, and incorporate aerosol indirect effects to enable a more comprehensive assessment of aerosol-cloud-radiation interactions and their influence on surface solar radiation.

CRediT authorship contribution statement

Jung-Woo Yoo: Writing – review & editing, Writing – original draft, Software, Methodology, Investigation, Formal analysis, Data curation, Conceptualization. **Soon-Young Park:** Validation, Methodology, Data curation. **Jiseon Kim:** Investigation, Data curation. **Hyun-Goo Kim:** Formal analysis. **Soon-Hwan Lee:** Writing – review & editing, Supervision, Investigation, Funding acquisition, Conceptualization.

Declaration of competing interest

The authors declare that they have no known competing financial interests or personal relationships that could have appeared to influence the work reported in this paper.

Acknowledgements

This research was supported by the Basic Science Research Program through the National Research Foundation of Korea (NRF), funded by the Ministry of Education (RS-2020-NR049592) and the Korean Government (MSIT) (RS-2022-NR070051).

Appendix A. Supplementary data

Supplementary data to this article can be found online at https://doi.org/10.1016/j.atmosres.2025.108295.

Data availability

Data will be made available on request.

References

Albrecht, B.A., 1989. Aerosols, clouds microphysics, and fractional cloudiness. Science 245 (4923), 1227–1230.

Berg, L.K., Kassianov, E.I., Long, C.N., Mills, D.L., 2011. Surface summertime radiative forcing by shallow cumuli at the atmospheric radiation measurement Southern Great Plains site. J. Geophys. Res. Atmos. 116, 1–13. https://doi.org/10.1029/2010JD014593.

Borenstein, S., 2008. The market value and cost of solar photovoltaic electricity production. CSEM Berkeley WP 176.

Charlson, R.J., Schwartz, S., Hales, J., Cess, R.D., Coakley, J.J., Hansen, J., Hofmann, D. J., 1992. Climate forcing by anthropogenic aerosols. Science 255 (5043), 423–430.

Che, H., Qi, B., Zhao, H., Xia, X., Eck, T.F., Goloub, P., Dubovik, O., Estelles, V., Cuevas-Agulló, E., Blarel, L., Wu, Y., Zhu, J., Du, R., Wang, Y., Wang, H., Gui, K., Yu, J., Zheng, Y., Sun, T., Chen, Q., Shi, G., Zhang, X., 2018. Aerosol optical properties and direct radiative forcing based on measurements from the China Aerosol Remote Sensing Network (CARSNET) in eastern China. Atmos. Chem. Phys. 18, 405–425. https://doi.org/10.5194/acp-18-405-2018.

de Andrade, R.C., Tiba, C., 2016. Extreme global solar irradiance due to cloud enhancement in northeastern Brazil. Renew. Energy 86, 1433–1441. https://doi.org/10.1016/j.renene.2015.09.012.

Demko, J.C., Geerts, B., Miao, Q., Zehnder, J.A., 2009. Boundary layer energy transport and cumulus development over a heated mountain: an observational study. Mon. Weather Rev. 137, 447–468. https://doi.org/10.1175/2008MWR2467.1.

Dumka, U.C., Kosmopoulos, P.G., Ningombam, S.S., Masoom, A., 2021. Impact of aerosol and cloud on the solar energy potential over the central gangetic himalayan region. Remote Sens. 13. https://doi.org/10.3390/rs13163248.

Eastman, R., Warren, S.G., 2014. Diurnal cycles of cumulus, cumulonimbus, stratus, stratocumulus, and fog from surface observations over land and ocean. J. Clim. 27, 2386–2404. https://doi.org/10.1175/JCLI-D-13-00352.1.

Emck, P., Richter, M., 2008. An upper threshold of enhanced global shortwave irradiance in the troposphere derived from field measurements in tropical mountains. J. Appl. Meteorol. Climatol. 47, 2828–2845. https://doi.org/10.1175/2008JAMC1861.1.

Emery, C.A., Tai, E., Yarwood, G., 2001. Enhanced meteorological modeling and performance evaluation for two Texas ozone episodes. In: Prepared for the Texas Natural Resource Conservation Commission. ENVIRON International Corporation, Novato, CA.

He, Z., Libois, Q., Villefranque, N., Deneke, H., Witthuhn, J., Couvreux, F., 2024. Combining observations and simulations to investigate the small-scale variability of surface solar irradiance under continental cumulus clouds. Atmos. Chem. Phys. 24, 11391–11408. https://doi.org/10.5194/acp-24-11391-2024.

Jun, M.J., Gu, Y., 2023. Effects of transboundary $PM_{2.5}$ transported from China on the regional $PM_{2.5}$ concentrations in South Korea: a spatial panel-data analysis. PLoS One 18, e0281988. https://doi.org/10.1371/journal.pone.0281988.

Kim, Y.P., Lee, G., 2018. Trend of air quality in Seoul: policy and science. Aerosol Air Qual. Res. 18, 2141–2156. https://doi.org/10.4209/aaqr.2018.03.0081.

Korras-Carraca, M.B., Gkikas, A., Matsoukas, C., Hatzianastassiou, N., 2021. Global clear-sky aerosol speciated direct radiative effects over 40 years (1980-2019). Atmosphere 12 (10), 1254. https://doi.org/10.3390/atmos12101254.

L'Ecuyer, T.S., Hang, Y., Matus, A.V., Wang, Z., 2019. Reassessing the effect of cloud type on earth's energy balance in the age of active spaceborne observations. Part I: top of atmosphere and surface. J. Clim. 32, 6197–6217. https://doi.org/10.1175/JCLI-D-18-0753.1.

Lee, H.J., Jo, Y.J., Kim, S., Kim, D., Kim, J.M., Choi, D., Jo, H.Y., Bak, J., Park, S.Y., Jeon, W., Kim, C.H., 2022. Transboundary aerosol transport process and its impact on aerosol-radiation-cloud feedbacks in springtime over Northeast Asia. Sci. Rep. 12, 4870. https://doi.org/10.1038/s41598-022-08854-1.

Li, Junjun, Lu, C., Chen, J., Zhou, X., Yang, K., Li, Jian, Wu, X., Xu, X., Wu, S., Hu, R., He, X., Zhou, Z., Zhu, L., Luo, S., 2024. The influence of complex terrain on cloud and precipitation on the foot and slope of the southeastern Tibetan Plateau. Clim. Dyn. 62, 3143–3163. https://doi.org/10.1007/s00382-023-07056-3.

Liu, M., Zhang, J., Shi, H., Fu, D., Xia, X., 2022. Data-driven estimation of cloud effects on surface irradiance at Xianghe, a suburban site on the North China Plain. Adv. Atmos. Sci. 39, 2213–2223. https://doi.org/10.1007/s00376-022-1414-x.

Miao, Y., Guo, J., Liu, S., Liu, H., Li, Z., Zhang, W., Zhai, P., 2017. Classification of summertime synoptic patterns in Beijing and their associations with boundary layer structure affecting aerosol pollution. Atmos. Chem. Phys. 17, 3097–3110. https://doi.org/10.5194/acp-17-3097-2017.

Oh, M., Kim, C.K., Kim, B., Yun, C., Kim, J.Y., Kang, Y., Kim, H.G., 2022. Analysis of minute-scale variability for enhanced separation of direct and diffuse solar irradiance components using machine learning algorithms. Energy 241, 122921. https://doi.org/10.1016/j.energy.2021.122921.

Oh, M., Kim, C.K., Kim, B., Kim, H.G., 2024. A novel model to estimate regional differences in time-series solar and wind forecast predictability across small regions: a case study in South Korea. Energy 291, 130284. https://doi.org/10.1016/j.energy.2024.130284.

Papachristopoulou, K., Fountoulakis, I., Gkikas, A., Kosmopoulos, P.G., Nastos, P.T., Hatzaki, M., Kazadzis, S., 2022. 15-year analysis of direct effects of total and dust aerosols in solar radiation/energy over the mediterranean basin. Remote Sens. 14. https://doi.org/10.3390/rs14071535.

Pfister, G., McKenzie, R.L., Liley, J.B., Thomas, A., Forgan, B.W., Long, C.N., 2003. Cloud coverage based on all-sky imaging and its impact on surface solar irradiance. J. Appl. Meteorol. 42, 1421–1434. https://doi.org/10.1175/1520-0450(2003)042<1421:CCBOAI>2.0.CO;2.

Pincus, R., Baker, M.B., 1994. Effect of precipitation on the albedo susceptibility of clouds in the marine boundary layer. Nature 372 (6503), 250–252.

Qu, Z., Oumbe, A., Blanc, P., Espinar, B., Gesell, G., Gschwind, B., Klüser, L., Lefèvre, M., Saboret, L., Schroedter-Homscheidt, M., Wald, L., 2017. Fast radiative transfer parameterisation for assessing the surface solar irradiance: the Heliosat-4 method. Meteorol. Z. 26, 33–57. https://doi.org/10.1127/metz/2016/0781.

Robbins, D., Poulsen, C., Siems, S., Proud, S., 2022. Improving discrimination between clouds and optically thick aerosol plumes in geostationary satellite data. Atmos. Meas. Tech. 15, 3031–3051. https://doi.org/10.5194/amt-15-3031-2022.

Song, Y., Chen, G., Wang, W.C., 2019. Aerosol direct radiative and cloud adjustment effects on surface climate over eastern China: analyses of WRF model simulations. J. Clim. 32, 1293–1306. https://doi.org/10.1175/JCLI-D-18-0236.1.

Tanesab, J., Parlevliet, D., Whale, J., Urmee, T., 2019. The effect of dust with different morphologies on the performance degradation of photovoltaic modules. Sustain. Energy Technol. Assessm. 31, 347–354. https://doi.org/10.1016/j.seta.2018.12.024.

Twomey, S., 1974. Pollution and the planetary albedo. Atmos. Environ. (1967) 8 (12), 1251–1256.

Wild, M., 2009. Global dimming and brightening: a review. J. Geophys. Res. Atmos. 114, 1–31. https://doi.org/10.1029/2008JD011470.

Wong, D.C., Pleim, J., Mathur, R., Binkowski, F., Otte, T., Gilliam, R., Pouliot, G., Xiu, A., Young, J.O., Kang, D., 2012. WRF-CMAQ two-way coupled system with aerosol feedback: Software development and preliminary results. Geosci. Model Dev. 5, 299–312. https://doi.org/10.5194/gmd-5-299-2012.

Yamasoe, M.A., do Rosário, N.M.E., Barros, K.M., 2017. Downward solar global irradiance at the surface in São Paulo city-the climatological effects of aerosol and clouds. J. Geophys. Res. 122, 391–404. https://doi.org/10.1002/2016JD025585.

Yoo, J.W., Jeon, W., Park, S.Y., Park, C., Jung, J., Lee, S.H., Lee, H.W., 2019. Investigating the regional difference of aerosol feedback effects over South Korea using the WRF-CMAQ two-way coupled modeling system. Atmos. Environ. 218, 116968. https://doi.org/10.1016/j.atmosenv.2019.116968.

Yoo, J.W., Jeon, W., Lee, H.W., Mun, J., Lee, S.H., Park, S.Y., 2020. The impact of foreign SO_2 emissions on aerosol direct radiative effects in South Korea. Atmosphere 11 (9). https://doi.org/10.3390/ATMOS11090887.

Yoo, J.W., Park, S.Y., Jeon, W., Jung, J., Park, J., Mun, J., Kim, D., Lee, S.H., 2024. Understanding the physical mechanisms of $PM_{2.5}$ formation in Seoul, Korea: assessing the role of aerosol direct effects using the WRF-CMAQ model. Air Qual. Atmos. Health. https://doi.org/10.1007/s11869-024-01538-x.

Zhang, X., Tan, S.C., Shi, G.Y., Wang, H., 2019. Improvement of MODIS cloud mask over severe polluted eastern China. Sci. Total Environ. 654, 345–355. https://doi.org/10.1016/j.scitotenv.2018.10.369.

Zhang, X., Wang, H., Che, H.Z., Tan, S.C., Shi, G.Y., Yao, X.P., 2020. The impact of aerosol on MODIS cloud detection and property retrieval in seriously polluted East China. Sci. Total Environ. 711, 134634. https://doi.org/10.1016/j.scitotenv.2019.134634.

Zhang, Y., Gao, Y., Xu, L., Zhang, M., 2022. Quantification of aerosol and cloud effects on solar energy over China using WRF-Chem. Atmos. Res. 275, 106245. https://doi.org/10.1016/j.atmosres.2022.106245.